J Mater Sci (2015) 50:4258–4269
DOI 10.1007/s10853-015-8978-0

Deformation and fracture behaviour of electroplated Sn–Bi/Cu solder joints

Yingxin Goh[1] · A. S. M. A. Haseeb[1] · Haw Ling Liew[1] · Mohd Faizul Mohd Sabri[1]

Received: 16 December 2014 / Accepted: 15 March 2015 / Published online: 25 March 2015

Abstract This work utilizes the lap shear test to investigate the shear strength and fracture behaviour of electroplated and reflowed Sn–Bi/Cu lead-free solder joints. Particular emphasis is given on the effects of reflow temperature on the interrelationships among the interfacial intermetallic compound (IMC) morphology, shear strength and the fracture mechanism of the solder joints. Single-lap shear specimens are prepared by joining two commercially pure Cu substrates with electroplated Sn–Bi solder of about 50 μm thickness. The geometry of the lap shear specimen is designed to minimize the differences between far-field and actual responses of the solder. Three reflow temperatures (200, 230 and 260 °C) are used to investigate the effects of reflow temperature on the microstructure and shear strength of the solder. The specimens are loaded to failure at a strain rate of 4×10^{-4}/s. Elemental mapping of the fracture surface is performed with field emission scanning electron microscope coupled with energy dispersive X-ray spectroscopy. A reflow temperature of 200 °C yields prism-like interfacial IMC morphology, while higher reflow temperatures of 230 and 260 °C yield scallop-like interfacial IMC morphology. The shear strength and elastic energy release, U, of the solder joints increase with increasing reflow temperature. Fractographs of the failed joints suggest that the fracture mechanism is dependent on the interfacial IMC morphology, where solder joints with prism-like interfacial IMC fail within the bulk solder and solder joints with scallop-like interfacial IMC failed with a mixture of bulk and interfacial fracture.

✉ Yingxin Goh
gohyingxin@um.edu.my

A. S. M. A. Haseeb
haseeb@um.edu.my

Haw Ling Liew
hlliew@um.edu.my

Mohd Faizul Mohd Sabri
faizul@um.edu.my

[1] Department of Mechanical Engineering, Faculty of Engineering, University of Malaya, 50603 Kuala Lumpur, Malaysia

Introduction

The continual reduction in solder joint size and increasing integration in electronic packaging demands for the improvement in reliability of solder joints. The properties of the joints are highly dependent on the solder composition, substrate material, flux, soldering conditions, joint geometry and testing conditions [1–4]. Although there are numerous reports on the mechanical behaviour of the Sn-based solder joints [1, 2, 4–10], it is difficult to compare the results due to the complex interaction between the factors mentioned above. Recent interests in the Sn–58 wt.%Bi alloy as potential solder material [11–14] have prompted investigations on the mechanical behaviour of the bulk alloy itself, as well as on the soldered Sn–Bi joints. Different techniques have been employed to characterize the mechanical properties of Sn–Bi alloys, such as nanoindentation [11, 15], adhesion pull-off test [1] and lap shear tests [2, 5, 7, 16], where the latter being the most commonly used.

Suh et al. [5] investigated the effects of interfacial intermetallic compound (IMC) growth on the shear strength of electrodeposited Sn–Bi solder joints. Ageing period of less than 24 h resulted in an increase in maximum shear strength because the prism-like IMC with high surface roughness binds strongly to the bulk solder alloy, hence

giving rise to increased shearing resistance at the solder/IMC interface. However, as the ageing period increases, the maximum shear strength of the Sn–Bi solder joints decreases due to the increase in IMC thickness and flatness. Tomlinson and Fullylove [2] compared the shear strength and ductility of several Sn-based solders at different test temperatures (20 and 100 °C) and strain rates (0.05 and 50.0 mm min^{-1}). At room temperature and low strain rate, the shear strength of Sn–57Bi solder is comparable to that of Sn–3.5Ag and Sn–5Sb solders. However, at 100 °C and high strain rate, the shear properties of Sn–57Bi solder deteriorates. Raeder et al. [7] found that the shear strength of Sn–Bi/Cu solder joints is similar to that of Sn–Pb. It is also reported in the same work that an ageing period of 30 days results in stratification of Bi-rich phase at the interface, which in turn increases the strength of the solder joints. In the as-reflowed joints, fracture occurs through separation of the IMC/Sn-rich phase. After ageing, Bi-rich phase formed at the solder/IMC interface upon consumption of Sn during IMC growth. In the aged samples, fracture occurs by cleavage through the Bi-rich phase, resulting in an increase in joint strength and ductility.

A review of the existing literature, as described above, reveals that only a limited number of studies have been devoted to the understanding of the fracture behaviour of Sn–Bi solder joints. It has been found that information on the fractography and discussions on fracture mechanism of Sn–Bi/Cu joints are scarce. This paper therefore focuses on the fracture behaviour of eutectic Sn–Bi/Cu solder joints subjected to shear loading. The Sn–Bi solder alloy in this work is electrodeposited from a plating bath and method developed in the authors' previous studies [17]. The shear strength of electrodeposited eutectic Sn–Bi alloy is examined as a function of different reflow temperature to provide a better understanding on the effects of temperature on the solder joints. The geometry of the solder joints is designed to minimize the differences between far-field and nominal responses of the solder. The far-field response refers to the shear response measured by the equipment for the overall substrate-solder assembly, while the nominal response refers to the actual shear response in the solder. The cross-sectional area of the Cu/Sn–Bi/Cu lap shear joints is examined to study the effects of reflow temperature on the microstructure of IMC. The effects of reflow temperature, IMC morphology and shear strength are taken into account in the discussion of fracture mechanism of the joints.

Experimental

Lap shear specimens were prepared by joining two pieces of commercially pure 35 mm × 35 mm Cu plates of 5 mm thickness, with an overlap length of 5 mm. The joint geometry was designed with reference to a few literature and standards [9, 18, 19], to minimize the deformation and bending of Cu during lap shear tests, allowing more reliable far-field displacement data collection. The eutectic Sn–Bi solder alloy was electroplated onto both the Cu plates from previously developed electroplating process [17]. The electroplating bath was composed of 120 ml/L of methane sulphonic acid (CH_3SO_3H), 30 g/L of $SnSO_4$, 9 g/L of Bi_2O_3, 5 g/L of hydroquinone and 2 g/L of gelatin. The electroplating was performed at a current density of 18 mA cm^{-2} for a plating time of 30 min which resulted in a solder thickness of 25 μm on one face of the Cu plate. Water-soluble flux was applied on both electroplated Cu substrates prior to reflow. The two electroplated Cu plates were aligned and a slight pressure of about 0.5 MPa. Reflow of the joints was performed with a reflow oven (C.I.F. Forced Convection FT02), and a schematic reflow profile is shown in Fig. 1. The joints were pre-heated to a temperature of 150 °C and held for 3 min and then reflowed at three different temperatures of 200, 230 and 260 °C for 10 min. A long reflow period was applied to provide sufficient time for heat re-distribution due to the large size of the Cu substrate in this case. The samples were cooled in the oven for 15 min (default mode of the reflow oven) and later removed to be cooled at room temperature.

Figure 2 shows the schematic diagram of the reflowed solder joints. The reflowed joints (Fig. 2a) were cut into strips of 5 mm width using electric discharge machining (EDM). Seven samples are produced after cutting the joined Cu plates as illustrated in Fig. 2b. The preparation of at least five shear samples from a single bulk sample was in accordance with ASTM D1002-10. Specimens situated at the middle (numbered 2–6 in Fig. 2a) were mechanically tested, while the specimens at both ends (numbered 1 and 7) were used for microstructure investigations. Lap shear

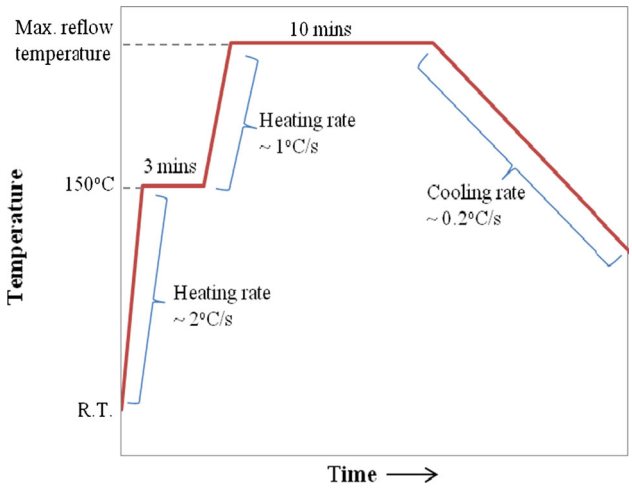

Fig. 1 Schematic reflow profile (*R.T.* room temperature; Maximum reflow temperature is 200, 230 or 260 °C)

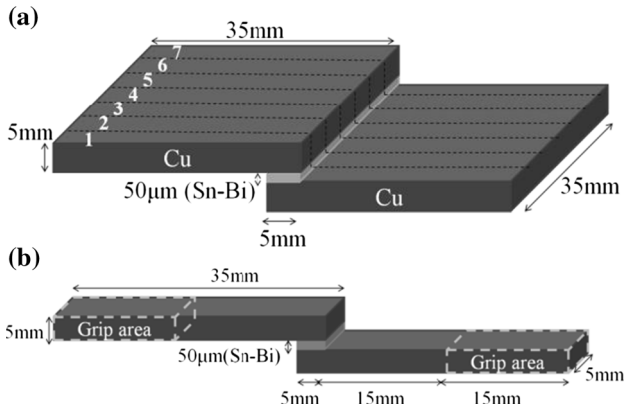

Fig. 2 Schematic diagram of **a** as-reflowed solder joint and **b** solder joint of 5 mm width machined with EDM

tests were performed at room temperature using the Instron 5848 MicroTester. Cross-sectional samples of as-reflowed Sn–Bi solder alloy joints were polished using standard metallographic procedures down to 0.04 μm colloidal silica suspensions. All cross-sectional samples were examined under a field emission scanning electron microscope (FESEM) (Auriga Zeiss Ultra-60) in the backscattered electron mode. The lap shear specimens were loaded to failure at a strain rate of 4×10^{-4}/s. The failed solder joints were kept carefully without damaging the fracture surface. Fractography was performed with FESEM (Quanta FEG 450) coupled with energy dispersive X-ray spectroscopy (EDX) (Oxford Instruments X-Max). Cross-sectional analysis of failed samples was performed with FESEM (Hitachi SU8030).

Results and discussion

Effects of reflow temperature on microstructure of solder joints

Representative micrographs of Cu/Sn–Bi/Cu solder joints reflowed at 200, 230 and 260 °C are shown in Fig. 3a–c, respectively. EDX point analysis showed that the lighter shade (white) regions are Bi-rich phase, while the darker shade (greyish) regions are Sn-rich phase. EDX area analysis was also performed on five randomly selected areas measuring 20 × 20 μm, and the average composition is found to be Sn–59.8 wt%Bi, which is near to the eutectic composition. Micrographs taken at a higher magnification at the Sn–Bi/Cu interface of the joints reflowed at 200, 230 and 260 °C are shown in Fig. 3d–f, respectively. Spot EDX analysis shows that the irregular layers form at the interface are Cu_6Sn_5 IMC, while the thin and flat layers are Cu_3Sn IMC. Figure 3d shows that the morphology of the interfacial Cu_6Sn_5 layer formed at a reflow temperature of 200 °C is of prism type. While the reflow temperatures of 230°C and 260 °C yield scallop-type interfacial IMC morphology (Fig. 3e, f). The nucleation and growth of IMC is highly dependent on the soldering temperature, cooling rate and concentration of Cu and Sn [20–22]. At a lower reflow temperature of 200 °C, the formation of prism-like IMC at the interface shows that nucleation is the dominant factor. While at higher temperatures of 230 and 260 °C, the formation of scallop-like IMC at the interface suggests that grain growth is the dominant factor. A very thin layer of Cu_3Sn IMC is also found between the Cu_6Sn_5 layer and the Cu substrate in all cases. The thickness of the Cu_3Sn layer increases with increasing reflow temperature.

It is also worth mentioning that there are some thickness variations for specimens reflowed at different temperatures. During joint preparation, pressure had to be applied to the joints at the reflow stage to improve adhesion and minimize void formation. But the applied pressure caused the molten solder to flow out of the joint area, resulting in a lower thickness as seen for the sample reflowed at 260 °C (Fig. 3c). These variations will be taken into account during discussion in the next section.

Effects of reflow temperature on shear strength of solder joints

The lap shear solder joints were loaded to failure in a tensile mode at a strain rate of 4×10^{-4}/s. Figure 4a shows the representative shear stress–shear–strain curve of samples taken from positions numbered 2–6 (Fig. 2). The elastic regime of the shear stress–shear strain curve of the solder joints is similar for all three reflow temperatures. This indicates that the shear modulus is not affected by varying the reflow temperature which is expected as the modulus is a structure insensitive property. Beyond the elastic regime, work hardening occurs in the solder joints until the maximum shear strength is reached, at which the solder joints fracture.

The average maximum shear strength shown in Fig. 4b is the average value from 15 samples, with the standard deviation shown as the error bar. It is found that the shear strength increases with increasing reflow temperature. During crack growth in metals, energy is expended by the formation of a new plastic zone at the tip of the advancing crack. The energy required for crack growth must be delivered as a release of the elastic energy. For stable crack growth, the energy release rate equals to the crack resistance of the material. If the energy release rate is larger than the crack resistance, crack instability occurs which leads to crack propagation and eventually fracture [23]. Hence, the higher the elastic energy release required for

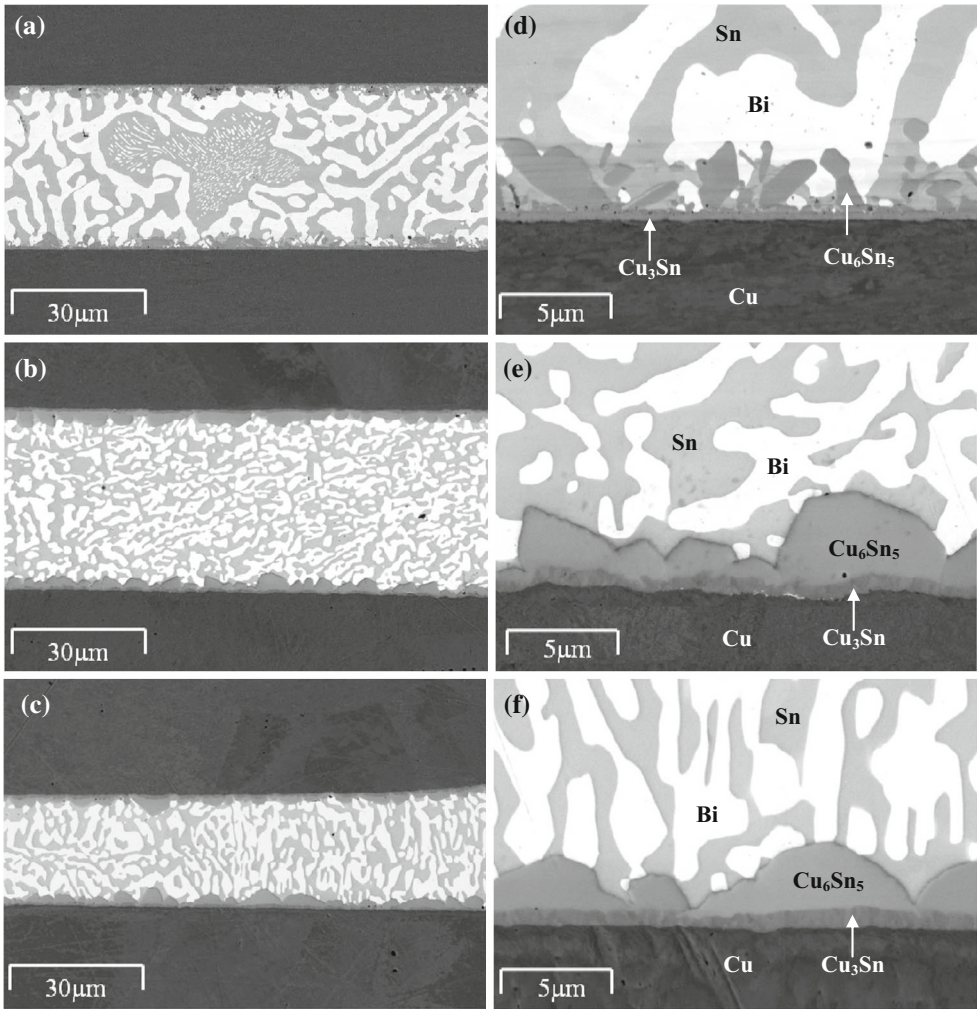

Fig. 3 Cu/Sn–Bi/Cu joint reflowed at **a** 200 °C, **b** 230 °C, **c** 260 °C, with the magnified micrograph of IMC morphology shown in (**d**, **e** and **f**), respectively

crack growth, the higher the crack resistance. The elastic energy release (per unit volume) required for crack propagation in Sn–Bi alloys, U, is calculated from the stress–strain curve for each reflow temperature and shown in Fig. 4a. A line parallel to the elastic zone of the curve is drawn from the fracture point to the x-axis. Another vertical line is extended from the fracture point to the x-axis to form a right-angled triangle. The area of the triangle indicates the elastic energy release per unit volume of solder. The elastic energy release increases by 225 % (from 960 to 2160 kJ m^{-3}) when reflow temperature is increased from 200 to 230 °C. This indicates an increase in the crack resistance of Sn–Bi solder joints. Sn–Bi solder joints reflowed at 260 °C yield a smaller elastic energy release increment of 150 % compared to joints reflowed at 230 °C (from 2160 to 3190 kJ m^{-3}). This suggests that the reflow temperature increment from 230 to 260 °C has a less profound effect on the crack resistance of the solder joints, compared to reflow temperature increment from 200 to 230 °C.

Table 1 shows the comparison of the shear properties of Sn–Bi/Cu lap shear solder joints reported in the literature. Values obtained in the present work are also shown in the last three rows of table for comparison. Comparing the work by Raeder et al. [7] and the present work (compare rows no. 1, 2 and 8), it is observed that at the same applied strain rate and same reflow temperature, the maximum shear strength value is rather comparable, regardless of the solder thickness and ageing period. The work of Tomlinson and Fullylove [2] employed a higher reflow temperature of 250 °C, and their reported shear strength and strain values are lower than those obtained in all other cases (rows no. 3 and 4). In the work of Tomlinson and Fullylove [2], when strain rate was increased from 8.3×10^{-5} to 8.3×10^{-2}, a drop in maximum shear strength is observed. This opposes the normal trend where lower strain rate should lead to lower maximum shear strength due to creep and stress relaxation effects. The authors concluded that Sn–57Bi joints often do not follow the general behaviour under different test conditions. Suh et al. [5] electrodeposited Sn–

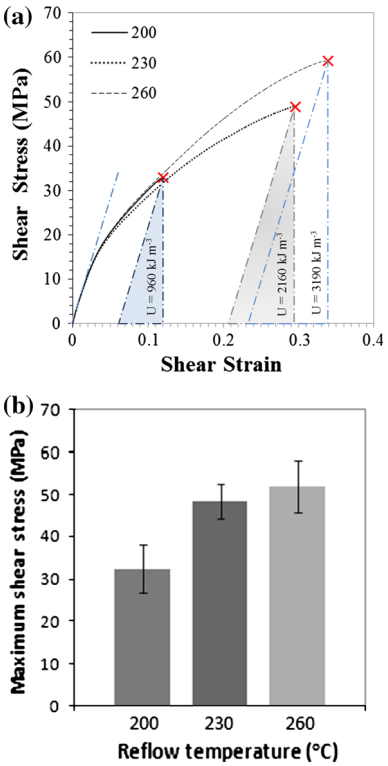

Fig. 4 **a** Shear stress–shear strain *curve* of samples reflowed at different temperatures and **b** the average maximum shear strength taken from 15 tests

58Bi solder and reflowed the joints under a slightly different reflow temperature of 220 °C and applied a slightly lower strain rate of 3.3×10^{-4}/s compared to our work (rows no. 5–7). For ageing period of less than 1 day, the maximum shear strength increased due to the bonding effect of prism-like IMC grains. As ageing time increases, the IMC layer thickened and flattened which caused the reduction in strength. Generally, the shear strength values of Sn–Bi/Cu solder joints obtained in this work are comparable to literature reports.

Fracture surface analysis of solder joints

To investigate how the IMC morphology affects the shear strength of solder joints in this work, Sn–Bi solder was chemically removed to reveal the IMC layer. Figure 5 shows the difference between IMC morphology of sample reflowed at 200 and 260 °C. The prism-like IMC morphology (Fig. 5a) may have provided a stronger binding effect to prevent the shearing at the interface. Yang et al. [22] studied the Cu_6Sn_5 morphology transition under different thermal conditions for the Sn–Ag/Cu system and the effects of the transition on the shear strength of the joints. Three types of interfacial IMC morphology were studied in their work: prism-like, scallop-like and layer-like. It is found that prism-like IMC binds stronger to the solder by penetrating into the solder matrix. As the binding effect increases the interfacial strength, the joints are more likely to fail in the bulk solder matrix. While for scallop-like and layer-like IMC structures, interfacial fracture is more dominant [22]. From Fig. 5b, it is seen that higher reflow temperature imposes a coarsening and flattening effect on the IMC grains. The scallop-like IMC morphology is more prone to shearing and crack initiation [22, 24]. The Sn–Bi/Cu joints soldered at 230 and 260 °C are likely to fail at the solder/IMC interface. Studies on the fracture surface are expected to give more insight on the shear behaviour of the solder joints.

Table 1 Comparison of shear properties of eutectic or near-eutectic Sn–Bi/Cu lap shear solder joints

Row no.	Solder preparation and thickness (μm)	Thermal history	Strain rate (s^{-1})	Maximum Shear Stress (MPa)	References
1	Sn–58.5Bi solder foil, 250 μm	Reflow at 200 °C, Aging at 80 °C (3 days)	4×10^{-4}	30	[25]
2	Sn–58.5Bi solder foil, 250 μm	Reflow at 200 °C, Aging at 80 °C (30 days)	4×10^{-4}	35 ± 1	
3	Sn–57Bi solder paste, 200 μm	Reflow at 250 °C (1 min)	8.3×10^{-5}	25.3 ± 2.6	[21]
4	Sn–57Bi solder paste, 200 μm	Reflow at 250 °C (1 min)	8.3×10^{-2}	19.6 ± 4.2	
5	Electrodeposited Sn–58Bi solder, 20–25 μm	Reflow at 220 °C	3.3×10^{-4}	41.9	[19]
6	Electrodeposited Sn–58Bi solder, 20–25 μm	Reflow at 220 °C Aging at 80 °C (1 day)	3.3×10^{-4}	47.8 ± 5.6	
7	Electrodeposited Sn–58Bi solder, 20–25 μm	Reflow at 220 °C, Aging at 80 °C (3 days)	3.3×10^{-4}	40.9 ± 5	
8	Electrodeposited Sn–59.8Bi solder, 39–42 μm	Reflow at 200 °C (10 min)	4×10^{-4}	32.4 ± 5.6	Present work
9	Electrodeposited Sn–59.8Bi solder, 39–42 μm	Reflow at 230 °C (10 min)	4×10^{-4}	48.4 ± 4.1	
10	Electrodeposited Sn–59.8Bi solder, 28–32 μm	Reflow at 260 °C (10 min)	4×10^{-4}	52.0 ± 6.1	

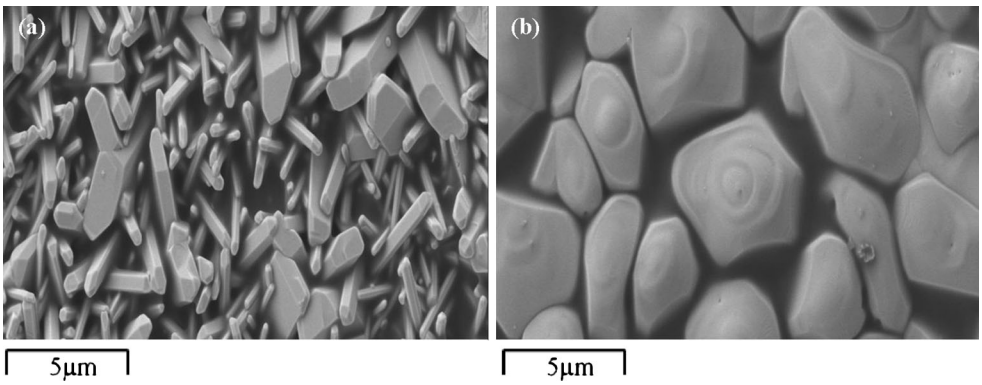

Fig. 5 Cu_6Sn_5 IMC morphology of Sn–Bi/Cu joints soldered at **a** 200 °C and **b** 260 °C

Figure 6a shows the representative micrograph of the fracture surface of solder joint reflowed at 200 °C. The fracture pattern is parallel to the shear direction. Under high magnification, the fracture surface reveals the presence of elongated dimples (Fig. 6b). This suggests that the fracture mode of this sample is ductile shear [23]. The spherical features found at the fracture surface (indicated by arrows) are voids caused by entrapped gas within the solder. Elemental mapping was performed to determine the elemental distribution at the fracture surface (Fig. 6c). Bi is mapped in green colour (Fig. 6c), while Sn is mapped in red (Fig. 6d). The composite map (Fig. 6e) shows some yellowish regions which are merely the mixture of green and red colour, indicating the mixture of both Bi and Sn phases. The absence of Cu in the elemental mapping data indicates no sign of exposed IMC from the elemental maps throughout the fracture surface. This can be related to the previous discussions on prism-like IMC morphology of joints reflowed at 200 °C, where the high surface area of IMC grains binds strongly to the bulk solder and avoid shearing at the joint interface.

A representative micrograph of samples reflowed at 230 °C shows an irregular area with darker shade (Fig. 7a). Such areas have been observed to cover about 25 % of the 5 × 5 mm fracture surface area. These areas are irregular in shape and are not due to void formation caused by gas entrapment. Under higher magnifications, the irregular area with darker shade shows granular features (Fig. 7b), and areas with brighter shade show fracture patterns that follow the shear direction (Fig. 7c). For elemental mapping, Bi is mapped in green colour (Fig. 7d), Sn is mapped in red colour (Fig. 7e) and Cu is mapped in blue colour (Fig. 7f).

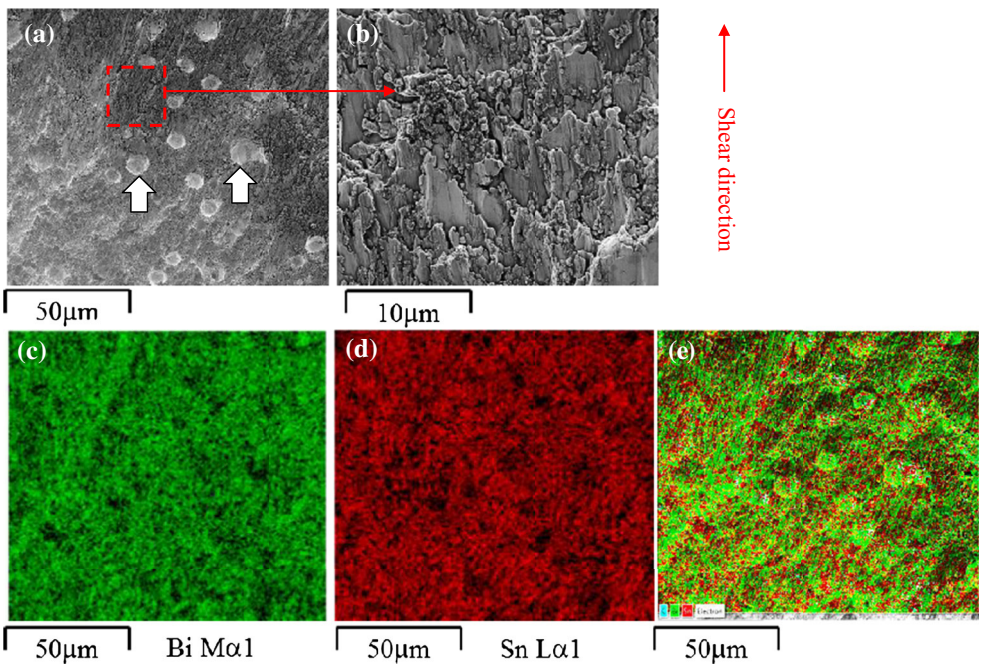

Fig. 6 **a** Micrograph **b** Magnified micrograph **c** Bi element mapping **d** Sn element mapping **e** composite mapping of fracture surface of joint reflowed at 200 °C

Shades of magenta colour are seen at the middle of the irregular area from the EDX mapping micrograph in Fig. 7d. Basically, Cu is exposed at the area along with Sn, with low intensity of Bi counts as seen in the individual colour maps (indicated by arrows). This indicates that there is interfacial fracture with exposure of Cu_6Sn_5 grains. The occurrence of interfacial fracture in samples reflowed at 230 °C could be due to the transformation of IMC morphology from prism-like to scallop-like structure. Scallop-like IMC grains have a lower surface roughness and have less ability to resist shearing. However, in our work, interfacial fracture covers only about 25 % of the fracture area, while the remaining area fails with ductile shear within the solder. Maximum shear strength values obtained (Fig. 4) show that there is a remarkable increase in shear strength and elastic energy release, U, when reflow temperature is increased from 200 to 230 °C. It may be inferred that the propagation of fracture from the interface to the bulk solder, and vice versa, has increased the shear strength and U.

Figure 8a depicts fractograph of solder joint reflowed at 260 °C. It is notable that the surface consists of sharp-edged features, some irregular areas (similar to joints reflowed at 230 °C), and the fracture patterns deviated from the shear direction. Fracture paths at different depths are observed from the magnified micrograph (Fig. 8b). Figure 8c shows a magnified view of fracture features that are parallel to the shear direction. But at the lower left corner, features show deviation from the shear direction. The sharp-edged features are Bi-rich phases (mapped in green, Fig. 8d) and are deviated from the shear direction, while Sn-rich phases (mapped in red, Fig. 8e) are found to follow the original shear direction. The main observation of the fractured joints reflowed at 260 °C is that the Bi-rich phase is seen to serve as a boundary to prevent the Sn-rich phase from sliding through during shear (indicated by arrows). At higher reflow temperature, Bi-rich phase has much higher tendency to coarsen. It is reported that coarsening can lead to adverse effects on the reliability of the solder joints because the Bi-rich phase is more brittle than the Sn-rich phase [1, 7, 25, 26]. However, in this work, Bi-rich phases do not seem to coarsen with increasing reflow temperature (Fig. 3), and the maximum shear strength is higher compared to lower reflow temperatures. On the other hand, it is apparent that the deviation in shear direction prolonged the fracture path of the joints, hence resulting in a higher U value.

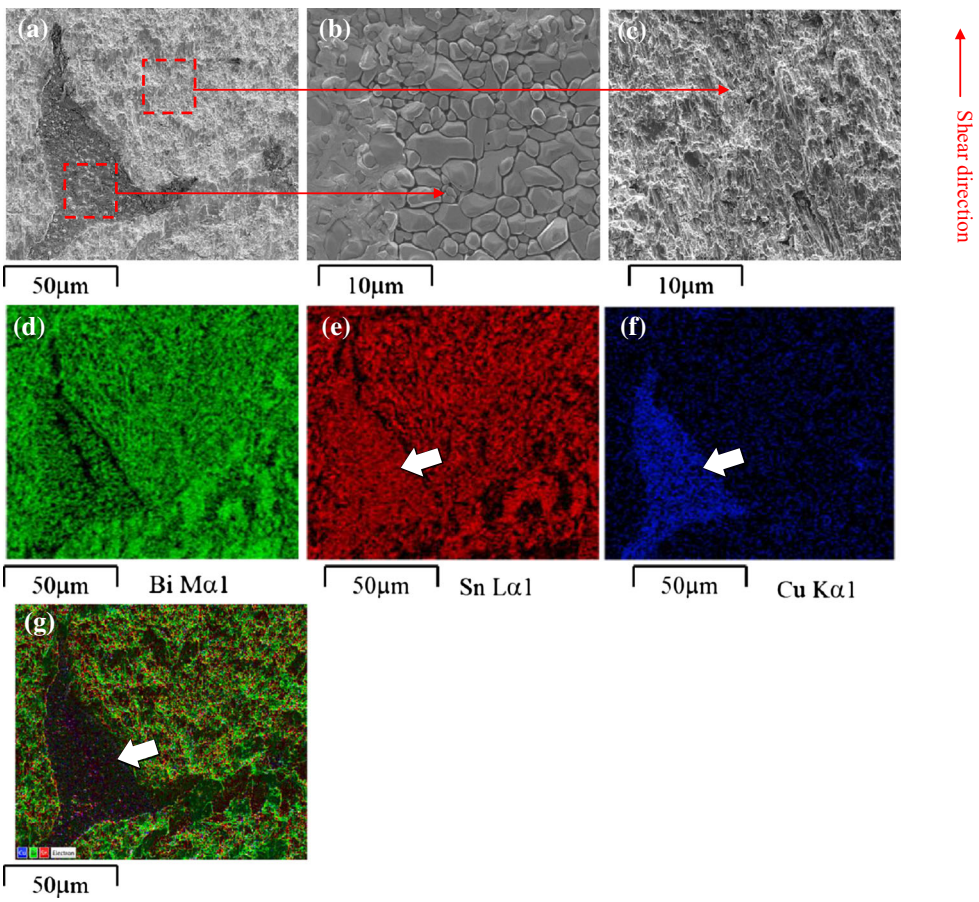

Fig. 7 **a** Micrograph **b**, **c** Magnified micrograph **d** Bi element mapping **e** Sn element mapping **f** Cu element mapping **g** composite mapping of fracture surface of joint reflowed at 230 °C

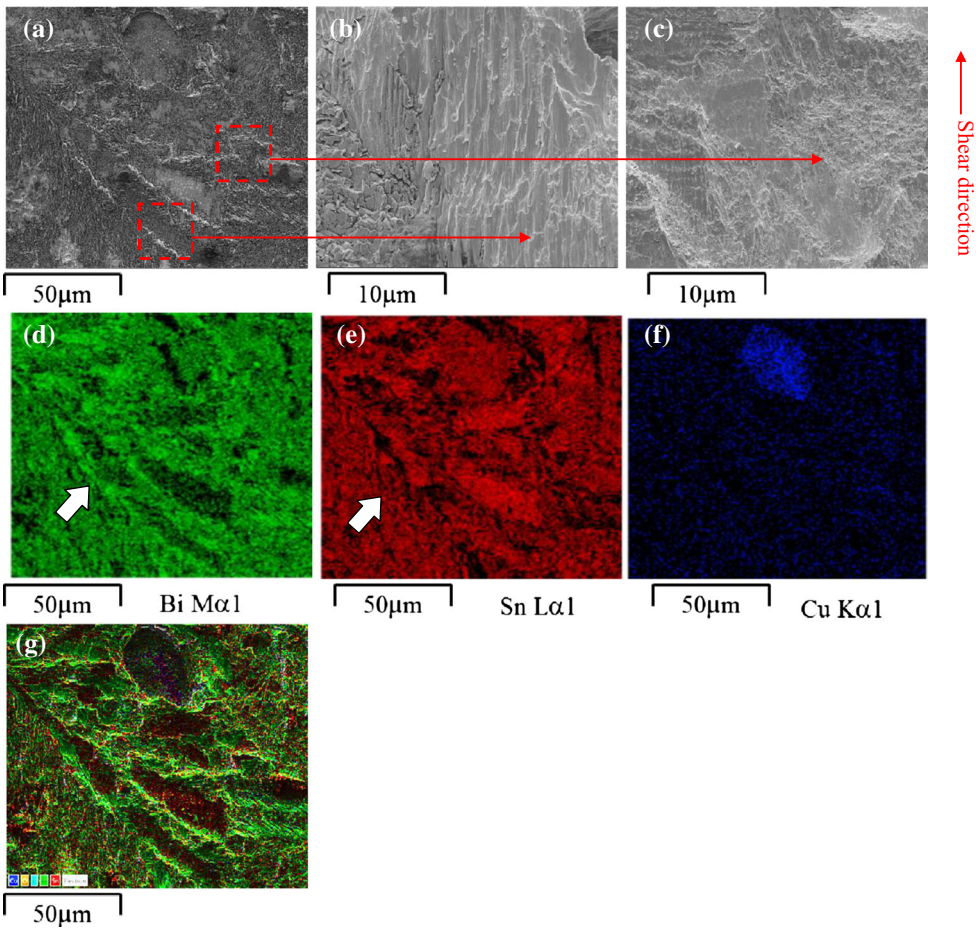

Fig. 8 **a** Micrograph **b**, **c** Magnified micrograph **d** Bi element mapping **e** Sn element mapping **f** Cu element mapping **g** composite mapping of fracture surface of joint reflowed at 260 °C

The cross-sectional views of the fractured solder joints were examined to provide a better insight into the fracture mode. Figure 9 shows the cross-sectional view of a representative fracture site of solder joints reflowed at 200 °C. The joints are observed to have failed within the bulk solder with very slight changes in fracture path. This is consistent with earlier suggestions, where samples reflowed at 200 °C tend to fail within the bulk solder. This could be due to the prism-like IMC morphology that formed at 200 °C bonds stronger to the solder matrix because of higher interfacial area. The crack initiation and propagation then occur within the bulk solder. The ease of crack propagation, without much change in fracture path, resulted in a relatively lower U value.

Figure 10 shows the cross-sectional view of the failed solder joints reflowed at 230 °C. Figure 10a is the micrograph taken at the edge of one of the failed samples. The scallop-like IMC grains became preferred crack initiation sites due to their low shear resistance [22, 24]. However, the crack propagation path changes when Bi-rich (light colour) phases are encountered (indicated with arrow). The micrographs of failed joints (Fig. 10b, c) show that the fracture path tends to propagate from bulk solder to IMC

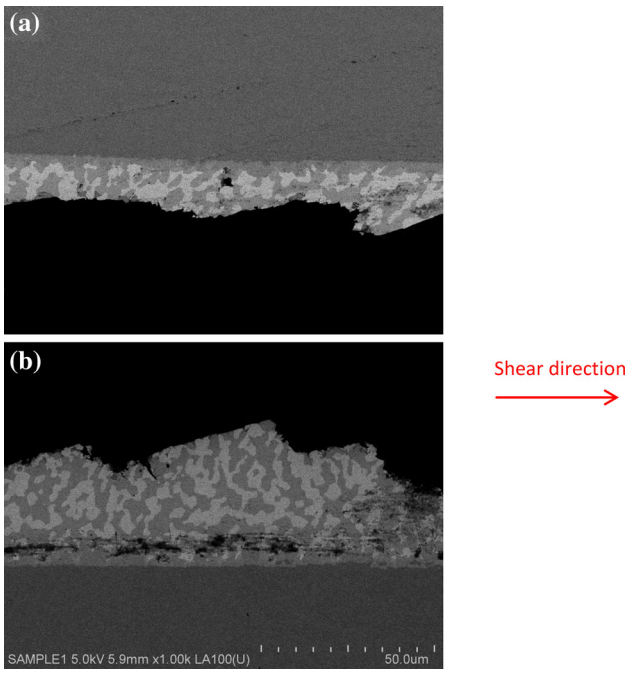

Fig. 9 Cross-sectional FESEM view of fractured solder joints reflowed at 200 °C **a** *top half* **b** *bottom half*

and vice versa. This mode of propagation of fracture is suggested to give rise to the higher U value for these samples.

A representative fracture site of failed solder joints reflowed at 260 °C is shown in Fig. 11. Similar to the samples reflowed at 230 °C, the samples reflowed at 260 °C also show propagation of fracture path from bulk solder to IMC and vice versa. This could be due to the same scallop-like IMC morphology formed at higher reflow temperatures. These IMC grains became preferred crack initiation sites, and fracture propagates along the IMC layer until some point. Abrupt changes in fracture path are observed for the solder joints reflowed at 260 °C (indicated with arrow).

Micrographs taken at another representative fracture site of solder joints reflowed at 260 °C show the mixture of bulk solder and interfacial fracture. It can be seen in Fig. 12a that the fracture proceeds along the Bi-rich phase within the bulk solder. When the Bi-rich phase in this eutectic structure approached the solder/IMC interface, the fracture path also propagates towards the IMC (indicated with arrow no.1). The magnified view where the crack propagates to the interface is shown in Fig. 12b. Fracture then proceeds along the solder/IMC interface for a short distance, before the fracture path propagates back into the solder matrix. This change in fracture path is seen to occur when the crack encounters another Bi-rich phase (indicated with arrow no. 2, magnified view in Fig. 12c). This phenomenon is observed only in solder joints reflowed at 230 and 260 °C.

The trend observed from the shear stress–strain curves and fractography suggests that the fracture behaviour of these Sn–Bi/Cu joints is dependent on the IMC morphology. A schematic diagram of possible fracture path is shown in Fig. 13. The schematic representation of joints reflowed at 200 °C (Fig. 13a) shows that the prism-like IMC layers, having a higher surface area, bound on to the bulk solder more effectively and avoid fracture along the interface. The flat fracture surface with dimpled features and the absence of Cu in elemental mapping (Fig. 6) indicate that the joints are sheared through the bulk solder without significant deviation in fracture path. The smooth fracture path of solder joints reflowed at 200 °C indicates poorer crack resistance, hence resulting in a lower shear strength and U value.

Figure 13b is the schematic representation for joints reflowed at 230 and 260 °C where both reflow

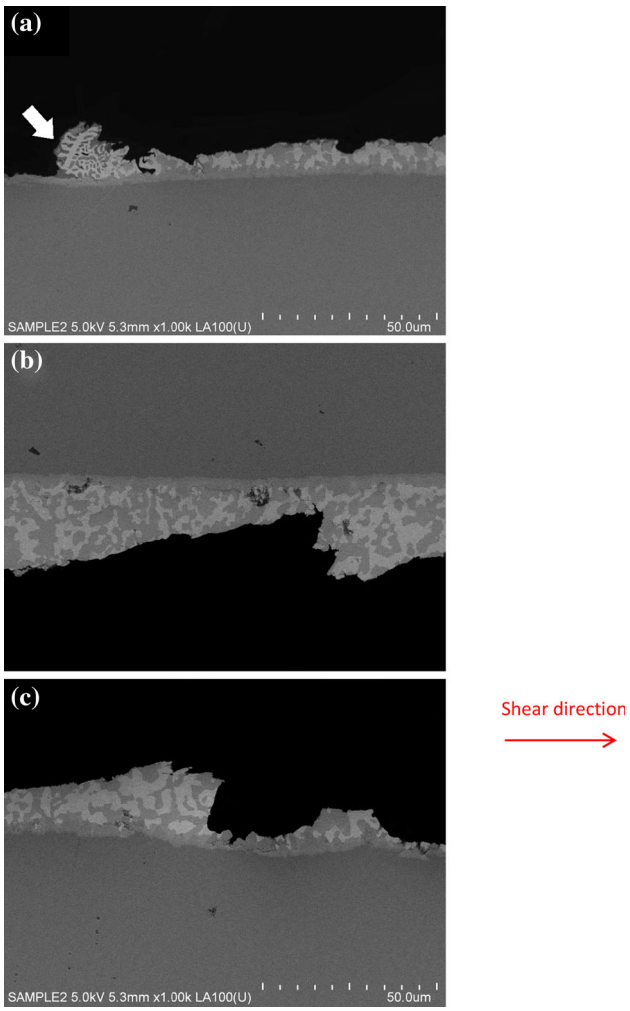

Fig. 10 Cross-sectional FESEM view of fractured solder joints reflowed at 230 °C **a** at the edge of bottom half **b** *top half* **c** *bottom half*

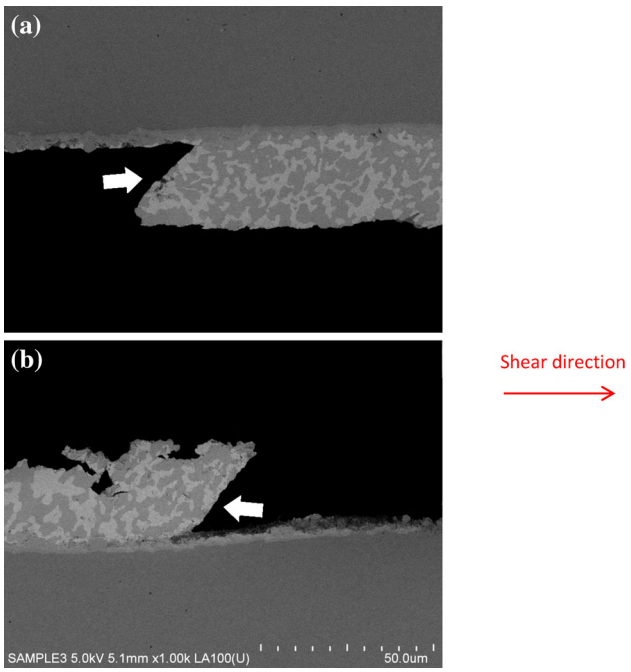

Fig. 11 Cross-sectional FESEM view of fractured solder joints reflowed at 260 °C **a** *top half* **b** *bottom half*

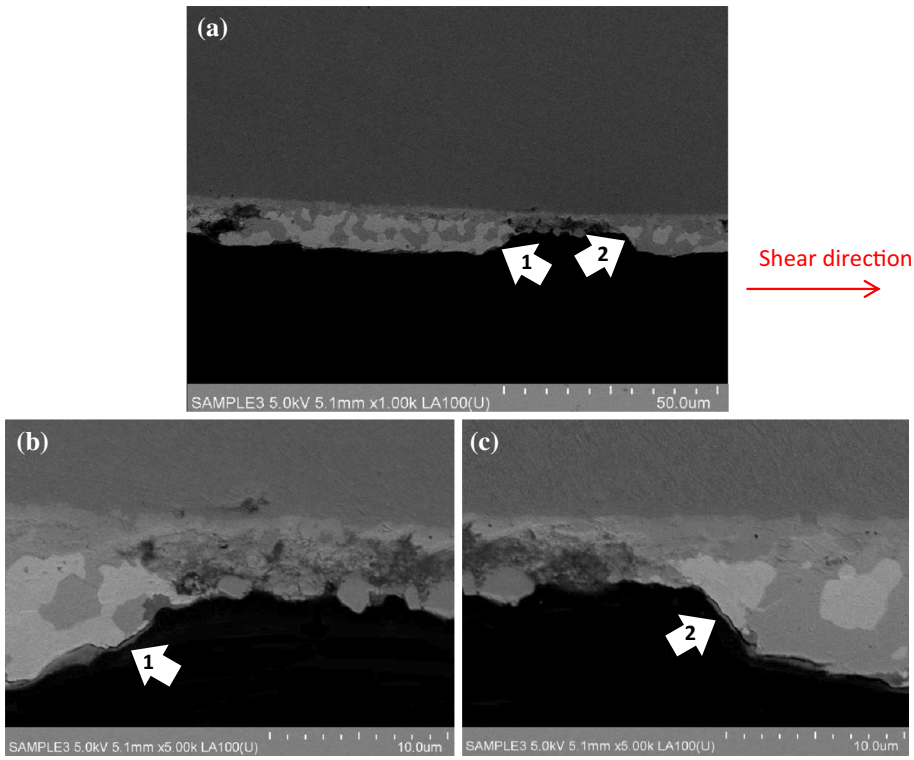

Fig. 12 **a** Representative fracture site of solder joint reflowed at 260 °C **b**, **c** magnified view of crack propagation

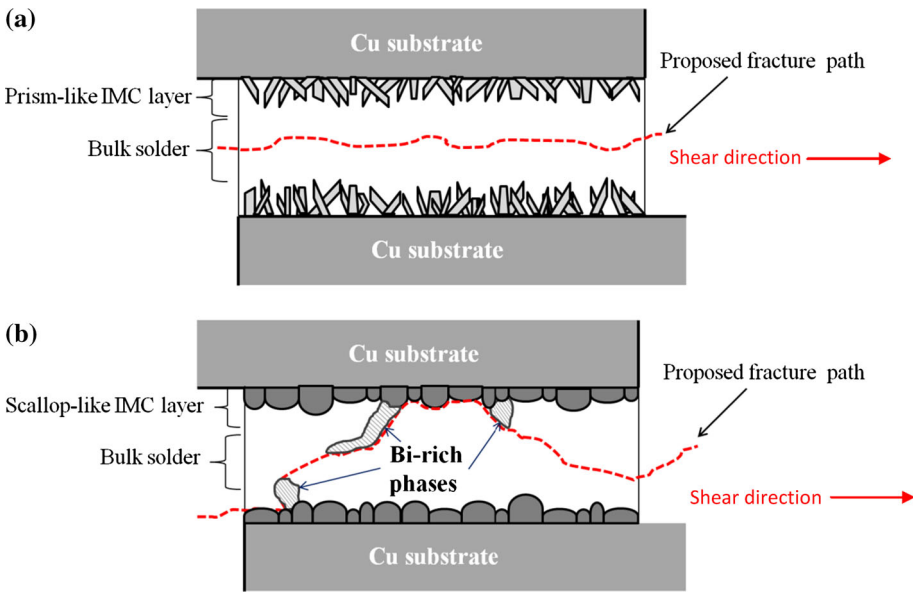

Fig. 13 Proposed fracture propagation **a** within bulk solder for joints reflowed at 200 °C and **b** with mixture of interfacial and bulk solder shearing for joints reflowed at 230 and 260 °C (not to scale)

temperatures yield scallop-like IMC morphology. The scallop-like structure has lower shear resistance which may promote interfacial crack initiation and fracture [22, 24]. However, it may be suggested that the eutectic Sn–Bi alloy may be hardened when this alloy is reflowed and soaked at a higher temperature. This alloy hardening effect may be attributed to the precipitation of hard Bi out of the super-saturated Sn-rich phase. The hard Bi-rich phases (shown in Fig. 13b) provide a hardening and blocking effect, similar to that of a second phase particle and interstitial hardening effect. This hardening effect increases the crack resistance of the solder joints, thus the crack propagation direction deviates from the original shear direction as can be seen from the fractographs in Figs. 8 and 12. In some cases, the abrupt change in fracture path (Fig. 11) is not along the Bi-rich phase entirely but a mixture of the phases. This may be related to the precipitation of hard Bi out of the super-saturated Sn-rich phase as suggested by Miyazawa and

Ariga [27]. There might be small Bi precipitates in the Sn-rich phase which provide the hardening effect to effectively deviate the fracture path. From the observations, it may be suggested that joints with scallop-like IMC morphology are prone to fail at the solder/IMC interface. However, the eutectic Sn–Bi alloy may have hardened when reflowed at higher temperatures. This leads to crack propagation from solder/IMC interface to bulk solder when the crack tip encountered Bi-rich phase. The diversion of fracture path resulted in a higher elastic energy release and higher shear strength of solder joints reflowed at higher temperatures.

Conclusions

The shear strength and fracture behaviour of electroplated Sn–Bi solders on Cu substrates were investigated in this work. Cross-sectional observations revealed that different interfacial IMC morphology was obtained at different reflow temperature. A reflow temperature of 200 °C yields prism-like interfacial IMC morphology, while 230 and 260 °C yield scallop-like IMC morphology. The maximum shear strength and elastic energy release (crack resistance) increase with increasing reflow temperature. Fractography of the failed joints showed that the fracture mechanism changes from dimpled fracture of bulk solder for joints reflowed at 200 °C, to mixture of interfacial and bulk solder fracture for joints reflowed at 230 and 260 °C. The difference in fracture behaviour is attributed mainly to the different reflow temperature and interfacial IMC morphology. For solder joints with prism-like IMC morphology, the higher surface area of IMC resulted in stronger bonding near the interface, hence fracture occurs rather smoothly across the bulk solder. Scallop-like IMC grains having less resistance to shearing are suggested to be crack initiation sites. Solder joints with scallop-like IMC are prone to fail at the solder/IMC interface first, but the Bi-rich phase near the interface provides hardening effect and deviates the fracture path. The crack propagation from solder/IMC interface to bulk solder and vice versa resulted in a higher shear strength and elastic energy release.

Acknowledgement This research is financially supported by the University of Malaya High Impact Research Grant (HIRG) No. UM.C/HIR/MOHE/ENG/26 (D000026-16001).

References

1. Miao HW, Duh JG, Chiou BS (2000) Thermal cycling test in Sn–Bi and Sn–Bi–Cu solder joints. J Mater Sci Mater Electron 11(8):609–618. doi:10.1023/A:1008928729212
2. Tomlinson WJ, Fullylove A (1992) Strength of tin-based soldered joints. J Mater Sci 27(21):5777–5782. doi:10.1007/Bf01119737
3. Yang LM, Zhang QK, Zhang ZF (2012) Effects of solder dimension on the interfacial shear strength and fracture behaviors of Cu/Sn–3Cu/Cu joints. Scr Mater 67(7–8):637–640. doi:10.1016/j.scriptamat.2012.07.024
4. Deng X, Sidhu RS, Johnson P, Chawla N (2005) Influence of reflow and thermal aging on the shear strength and fracture behavior of Sn–3.5Ag Solder/Cu joints. Metall Mater Trans A 36A(1):55–64. doi:10.1007/s11661-005-0138-8
5. Suh MS, Park CJ, Kwon HS (2008) Growth kinetics of Cu-Sn intermetallic compounds at the interface of a Cu substrate and 42Sn–58Bi electrodeposits, and the influence of the intermetallic compounds on the shear resistance of solder joints. Mater Chem Phys 110(1):95–99. doi:10.1016/j.matchemphys.2008.01.021
6. Felton LE, Raeder CH, Knorr DB (1993) The properties of tin–bismuth alloy solders. JOM 45(7):28–32
7. Raeder CH, Felton LE, Tanzi VA, Knorr DB (1994) The effect of aging on microstructure, room-temperature deformation, and fracture of Sn–Bi/Cu solder joints. J Electron Mater 23(7):611–617. doi:10.1007/Bf02653346
8. Raeder CH, Mitlin D, Messler RW (1998) Modelling the creep rates of eutectic Bi–Sn solder using the data from its constitutive phases. J Mater Sci 33(18):4503–4508. doi:10.1023/A:1004439931547
9. Shen YL, Chawla N, Ege ES, Deng X (2005) Deformation analysis of lap-shear testing of solder joints. Acta Mater 53(9):2633–2642. doi:10.1016/j.actamat.2005.02.024
10. Nai SML, Wei J, Gupta M (2009) Interfacial intermetallic growth and shear strength of lead-free composite solder joints. J Alloy Compd 473(1–2):100–106. doi:10.1016/j.jallcom.2008.05.070
11. Roh M-H, Jung JP, Kim W (2014) Microstructure, shear strength, and nanoindentation property of electroplated Sn–Bi microbumps. Microelectron Reliab 54(1):265–271. doi:10.1016/j.microrel.2013.09.016
12. Goh Y, Haseeb ASMA, Sabri MFM (2013) Electrodeposition of lead-free solder alloys. Solder Surf Mt Technol 25(2):76–90. doi:10.1108/09540911311309031
13. Zhang L, Tu KN (2014) Structure and properties of lead-free solders bearing micro and nano particles. Mater Sci Eng 82:1–32. doi:10.1016/j.mser.2014.06.001
14. Goh Y, Lee SF, Haseeb ASMA (2013) Formation of Sn–Bi solder alloys by sequential electrodeposition and reflow. J Mater Sci Mater Electron 24(6):2052–2057. doi:10.1007/s10854-012-1055-4
15. Shen L, Septiwerdani P, Chen Z (2012) Elastic modulus, hardness and creep performance of SnBi alloys using nanoindentation. Mat Sci Eng A 558:253–258. doi:10.1016/j.msea.2012.07.120
16. Peng Y, Deng K (2015) Study on the mechanical properties of the novel Sn–Bi/Graphene nanocomposite by finite element simulation. J Alloys Compd 625:44–51. doi:10.1016/j.jallcom.2014.11.110
17. Goh Y, Haseeb ASMA, Sabri MFM (2013) Effects of hydroquinone and gelatin on the electrodeposition of Sn–Bi low temperature Pb-free solder. Electrochim Acta 90:265–273. doi:10.1016/j.electacta.2012.12.036
18. D1002-10 AS (2010) Standard test method for apparent shear strength of single-lap-joint adhesively bonded metal specimens by tension loading (metal-to-metal). ASTM International, West Conshohocken. doi: 10.1520/d1002-10
19. Siewert TA, Handwerker CA (2002) Test procedures for developing solder data. Vol 960-8. National Institute of Standards and Technology, Washington
20. Gu LY, Qu L, Ma HT, Luo ZB, Wang L (2011) Effects of soldering temperature and cooling rate on the as-soldered microstructures of intermetallic compounds in Sn–Ag/Cu joint. 2011 12th international conference on electronic packaging technology and high density packaging (Icept–Hdp), pp 342–345

21. Laurila T, Vuorinen V, Kivilahti JK (2005) Interfacial reactions between lead-free solders and common base materials. Mat Sci Eng R 49(1–2):1–60. doi:10.1016/j.mser.2005.03.001
22. Yang M, Li M, Wang L, Fu Y, Kim J, Weng L (2010) Cu6Sn5 morphology transition and its effect on mechanical properties of eutectic Sn–Ag solder joints. J Electron Mater 40(2):176–188. doi:10.1007/s11664-010-1430-y
23. Broek D (1996) Elementary engineering fracture mechanics. Kluwer, Dordrecht
24. Tu PL, Chan YC, Lai JKL (1997) Effect of intermetallic compounds on the thermal fatigue of surface mount solder joints. IEEE Trans Compon Packag B 20(1):87–93. doi:10.1109/96.554534
25. Huang ML, Wu CML, Lai JKL, Chan YC (2000) Microstructural evolution of a lead-free solder alloy Sn–Bi–Ag–Cu prepared by mechanical alloying during thermal shock and aging. J Electron Mater 29(8):1021–1026. doi:10.1007/s11664-000-0167-4
26. Felton L, Raeder C, Knorr D (1993) The properties of tin–bismuth alloy solders. JOM 45(7):28–32. doi:10.1007/bf03222377
27. Miyazawa Y, Ariga T (1999) Microstructural change and hardness of lead free solder alloys. In: First international symposium on environmentally conscious design and inverse manufacturing (EcoDesign '99), Tokyo, Japan. IEEE, pp 616–619